Université Grenoble Alpes

Laboratoire Kastler Brossel, Sorbonne Université

Master 1 internship

Characterization of optical & quantum properties of perovskite nanocrystals

Supervisor :
Alberto BRAMATI, Professor

Author :
Milino KEROWGODAGE

Referent teacher :
Nedjma BENDIAB, Professor

Second Marker :
Elisabeth CHARLAIX, Professor

Period of 4^{th} May 2021 to 30^{th} July 2021

Acknowledgments

I would like to thank all the people who contributed to the success of my internship and who helped me in writing this report.

First of all, I would like to warmly thank my supervisor, Prof. Alberto BRAMATI from the Kastler Brossel Laboratory (LKB), Sorbonne University who helped me a lot proposing this internship and allowed me to apply to the Nano Optics team of the Quantum Optics group at the LKB which investigates original approaches for coupling optical fibers and more generally waveguides to various solid-state quantum emitters.

I also thank Prof. Emmanuel LHUILLIER, research scientist at the Institut des Nanosciences de Paris (INSP) with whom we collaborated for the perovskite synthesis, the chemical experiments (resulats and analysis of the data obtained by the transmission electron microscopy (TEM) and the Synchrotron SOLEIL experiments) and for the nanocrystals (NCs) introduction lectures that he gave us during my internship.

Furthermore, I wanted to thank Marianna D'AMATO, PhD student at the LKB, Sorbonne University from the Nano Optics team with whom I worked during this internship and Chengjie DING, postdoctoral research fellow at the LKB, Sorbonne University for the time she devoted to me to explain her *Nanobright* project with the new building setup which is studied in the same team.

The time spent with Prof. Alberto BRAMATI, Marianna and Chengjie, sharing their expertise on a daily basis was a great help and even more in times of doubt.

I also wanted to thank the researchers, PhD students, postdoctoral research fellows and trainees of the other teams of the Quantum Optics group (Prof. Quentin GLORIEUX, Maxime JACQUET, Murad ABUZARLI, Tangui ALADJIDI, Thomas PICOT, Wei LIU, Kévin FALQUE, Ankul PRAJAPATI...) for their welcome, their kindness, their team spirit and their sharing about the research activities on which they are currently working on.

Thereby, I really enjoy to take part to the different activities proposed by the group such as the journal club but also all the moments when we spend time together at lunch, coffee break and many others which were rewarding from a human and scientific point of view.

Moreover, I thank the whole administrative and technical teams for their efficiency and communication for all the administration and technical tasks that I got during my internship.

Finally, I would like to specially thank again Murad and Hadriel MAMANN

(postdoctoral research fellow at the LKB, Sorbonne University on the Quantum Networks team) who tell me more about the LKB when I was asking advices from people who are working at this laboratory in order to apply for an internship.

Contents

Introduction

The theory of Quantum Mechanics was developed at the beginning of the XX^{th} century by physicists such as Planck, Einstein, Schrödinger and Dirac in order to provide a description of the physical properties of nature at the scale of atoms and subatomic particles not explained with a classical approach.

Nowadays, many applications based on knowledge coming from the quantum theory, creating and manipulating quantum states to process information have been developed such as quantum communication, quantum cryptography and quantum computing.

In order to implement these quantum technologies, we need quantum objects. Thus, single photons are a particular interest as they are ideal carriers for quantum information.

An ideal single photon source is defined by several criteria :

- The emission of a single photon ;
- The probability of emitting a single photon (equal to 1) and the probability of emitting multiple photon (equal to 0) ;
- The indistinguishability of the emitted photons ;
- The brightness and quantum yield (QY) [23] ;
- The arbitrarily fast repetition rate.

In the last years, systems [8] such as stochastic single photon generation or deterministic single photon sources (e.g single photon, single atoms, single ions, single molecules, semiconductor quantum dots (SC QDs), single color centers in diamonds [16] and nanodiamonds) were studied in order to produce a single photon emitter.

However, an interest in perovskite nanocrystals (NCs) firstly studied for solar-cell application was raising in the quantum optics community. It was demonstrated that quantum confined perovskite NCs can behave as very efficient single photon emitters at room temperature as there is a strong antibunching detection in photo-luminescence (PL) measurements [25].

Moreover, perovskite NCs are versatile emitters due to their tuning emission wavelength playing on their size and composition [18] and are easily synthesized by low-cost, well mastered wet chemistry techniques.

Yet, their use is limited by different instabilities as they usually bleach after few minutes under illumination and present fluctuations (blinking) on the PL intensity.

In this internship report, a full analysis of the optical and quantum properties of

highly efficient $CsZnPbBr_3$ doped and $CsZnPbBr_3 - PEI$[1] perovskite nanocubes (deterministic single photons sources) exhibiting reduced blinking and showing antibunching will be done.

These nanocubes are synthesized in collaboration with the Institut des Nanosciences de Paris (INSP) with a specific method, allowing us to obtain higher stable samples which can be excited under optical excitation for more than one hour and all the experiments which will be presented have been carried out at the Kastler Brossel Laboratory (LKB), Sorbonne University.

Here below are the main parts of this report :

- Chapter 1 : Reminder of the important theoretical notions for the optical and quantum characterization of a single photon source.
- Chapter 2 : Quick review of the structure and optical characteristics of caesium lead halide perovskites followed by a focusing on the perovskite NCs single photon emitters behaviour.
- Chapter 3 : Explanation of the experimental setup and the methods used to have access to the acquired information.
- Chapter 4 : Results and analysis of both optical and quantum properties of the $CsZnPbBr_3$ doped and $CsZnPbBr_3 - PEI$ NCs.
- Chapter 5 : Outlook and perspectives.

[1]Polyethylenimine (PEI) : Polymer with repeating unit of the amine group and two carbon aliphatic CH_2CH_2 spacer

Chapter 1

Single photon sources : theoretical reminder

1.1 Single photon emitters

Single photon emitters (SPEs) are objects that emit no more than one photon at each time.

Theoretically, the ideal single photon emitter is a two-level system : when it is excited from the ground state to the excited state, it needs a certain amount of time to relax again in the ground state while emitting a photon. Until this photon is emitted, it is not possible to excite it anymore. In our case, we have a multiple states system where carriers are excited out of resonance with an energetic light but the same process as a two-level system occurs at the end.

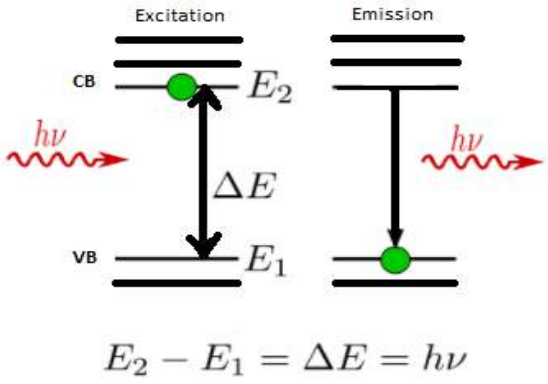

Figure 1.1: Scheme of a quantum emitter excited by a resonant monochromatic radiation. CB : Conduction band & VB : Valence band

Thus, the recombination of the excited carriers is divided into two parts : a radiative recombination, when the photon is emitted, and a non-radiative recombination when the excess energy is converted into heat by the emitted phonon.

This leads to the fact that the emitted photon is usually at a different wavelength than the excitation beam, allowing an easy way to separate photons by filtering the light using spectral selective optical elements.

1.2 Second-order autocorrelation function

In quantum optics, correlation functions are used to characterize the statistical and coherence properties of an electromagnetic field.

The correlation between pairs of fields, $g^{(2)}$ (also called intensity-intensity correlation), typically is used to find the statistical character of intensity fluctuations.

It is also used to differentiate between states of light that require a quantum mechanical description and those for which classical fields are sufficient.

1.2.1 Classical fields

In the classical theory framework, the normalized intensity correlation function is defined by [20] [9] :

$$g^{(2)}(\vec{r_1}, t_1, \vec{r_2}, t_2) = \frac{\langle E^*(\vec{r_1}, t_1) E^*(\vec{r_2}, t_2) E(\vec{r_1}, t_1) E(\vec{r_2}, t_2) \rangle}{\left\langle |E(\vec{r_1}, t_1)|^2 \right\rangle \left\langle |E(\vec{r_2}, t_2)|^2 \right\rangle} \tag{1.1}$$

With $\vec{E}$: the electric field, $\vec{r_i}$: the position coordinates and t_i : the times.

If $\vec{E}$ is a classical electric field, we have :

$$I(\vec{r}, t) = 2\varepsilon_0 c \, |E(\vec{r}, t)|^2 \tag{1.2}$$

With I : the light intensity and $|E(\vec{r}, t)|^2 = E^*(\vec{r}, t) E(\vec{r}, t)$.

Thus, for a plane parallel wave in a stationary state, the $g^{(2)}$ function will have the following form :

$$g^{(2)}(\tau) = \frac{\langle I(t) I(t+\tau) \rangle}{\langle I(t) \rangle^2} \tag{1.3}$$

With $\tau = t_1 - t_2$: the time delay between two photons arrival.

Properties :

1. $g^{(2)}(-\tau) = g^{(2)}(\tau)$: $g^{(2)}$ is an even function.

2. Allowed range of values (for both stationary and non stationary light beams) : $1 \leq g^{(2)}(0) \leq \infty$.

   Proof : Using the variance of the intensity (real number), we have :

   $\langle I^2(t) \rangle - \langle I(t) \rangle^2 = \left\langle [I(t) - \langle I(t) \rangle]^2 \right\rangle \geq 0$ (König-Huygens theorem)

   $\Leftrightarrow \langle I(t) \rangle^2 \leq \langle I^2(t) \rangle$ (Cauchy-Schwarz inequality).

   The second-order coherence for zero time delay satisfies : $1 \leq g^{(2)}(0)$.

   As it is not possible to establish any upper limit, the complete range of allowed value is given by : $1 \leq g^{(2)}(0) \leq \infty$.

   Furthermore, as the intensity is positive, for nonzero time delays, we have :

   $\forall \tau \neq 0, 0 \leq g^{(2)}(\tau) \leq \infty$.

3. For classical fields (for both stationary and non stationary light beams), we have : $g^{(2)}(\tau) \leq g^{(2)}(0)$.

   Proof : Using the Cauchy-Schwarz inequality to the intensities, we have :

   $\left[\sum_i \langle I(t_i)\rangle \langle I(t_i+\tau)\rangle\right]^2 \leq \left[\sum_i \langle I^2(t_i)\rangle\right]\left[\sum_i \langle I^2(t_i+\tau)\rangle\right]$ with $i \in \mathbb{N}^*$.

   For a sufficiently long and numerous series, the two summations on the right hand are equal.

   This latest assumption leads to :

   $\langle I(t)I(t+\tau)\rangle \leq \langle I^2(t)\rangle \Rightarrow g^{(2)}(\tau) \leq g^{(2)}(0)$.

4. If intensities are independent, we have : $\lim_{\tau\to\infty} g^2(\tau) = 1$.

1.2.2 Quantum fields

The prediction of $g^{(2)}$ change when the classical fields are replaced with quantum fields.

In the quantum theory framework, we have [20] [9] :

$$\begin{cases} E^* & \rightarrow & \hat{E}^- \\ E & \rightarrow & \hat{E}^+ \end{cases} \tag{1.4}$$

With $\hat{E}^- = -i\sqrt{\left(\frac{\hbar\omega}{2\varepsilon_0 V}\right)}\hat{a}^\dagger e^{-i(\vec{k}\cdot\vec{r}-\omega t)}$.

We will now assume stationary counting statistics. Thus, in this case, we have :

$$g^{(2)}(\tau) = \frac{\left\langle \hat{a}^\dagger(t)\hat{a}^\dagger(t+\tau)\hat{a}(t+\tau)\hat{a}(t)\right\rangle}{\left\langle \hat{a}^\dagger(t)\hat{a}(t)\right\rangle^2} \tag{1.5}$$

On one hand, for $\tau = 0$, we have :

$$g^{(2)}(0) = \frac{\left\langle \hat{a}^\dagger\hat{a}^\dagger\hat{a}\hat{a}\right\rangle}{\left\langle \hat{a}^\dagger\hat{a}\right\rangle^2} = \frac{\left\langle (\hat{a}^\dagger)^2\hat{a}^2\right\rangle}{\left\langle \hat{a}^\dagger\hat{a}\right\rangle^2} \tag{1.6}$$

This relation being the probability of detecting two simultaneous photons, normalized by the probability of detecting two photons at once for a random photon source.

On the other hand, the variance of the photon number operator is defined by :

$$\left\langle (\Delta\hat{n})^2\right\rangle = \left\langle \hat{n}^2\right\rangle - \left\langle \hat{n}\right\rangle^2 = \left\langle (\hat{a}^\dagger\hat{a})^2\right\rangle - \left\langle \hat{a}^\dagger\hat{a}\right\rangle \tag{1.7}$$

Using the commutator operators relations[1], we have :

$$\left\langle (\Delta\hat{n})^2\right\rangle = \left\langle (\hat{a}^\dagger)^2\hat{a}^2\right\rangle + \left\langle \hat{a}^\dagger\hat{a}\right\rangle - \left\langle \hat{a}^\dagger\hat{a}\right\rangle^2$$

$$\left\langle (\Delta\hat{n})^2\right\rangle - \left\langle \hat{n}\right\rangle = \left\langle (\hat{a}^\dagger)^2\hat{a}^2\right\rangle - \left\langle \hat{a}^\dagger\hat{a}\right\rangle^2 \tag{1.8}$$

[1] We use both the commutation relation between the creation and annihilation operators and the definition of the number operator given by these two ladder operators

Thereby, we have :

$$\frac{\langle(\Delta\hat{n})^2\rangle - \langle\hat{n}\rangle}{\langle\hat{n}\rangle^2} = g^{(2)}(0) - 1$$

$$g^{(2)}(0) = 1 + \frac{\langle(\Delta\hat{n})^2\rangle - \langle\hat{n}\rangle}{\langle\hat{n}\rangle^2} \tag{1.9}$$

Finally, for any arbitrary state, we have :

$$g^{(2)}(0) = 1 + \frac{\langle(\Delta n)^2\rangle - \langle n\rangle}{\langle n\rangle^2} \tag{1.10}$$

N.B : For more information about the semi-classical theory framework approach of the $g^{(2)}$ function, see the reference [34].

Remark : We can also use the quantum theory of coherence [11] to express the second-order autocorrelation function (using the density matrix operator).

Here below are the three distinguished light behaviour cases :

1) If $\lim_{\tau\to\infty} g^{(2)}(\tau) = 1 \Rightarrow g^{(2)}(0) > 1$: **bunched light** (for shorter time ranges, higher probability to detect a second photon) ;

2) $g^{(2)}(0) = 1$: **coherent light** (for all time ranges, same probability to detect a second photon) ;

3) $g^{(2)}(0) < 1$: **antibunched light** (for small time ranges, negligible probability to detect a second photon).

N.B : For more information about the photon statistics, see the reference [9].

Experimentally, the value of $g^{(2)}(0)$ that is measured, concludes on the quality of a single photon emitter. The smaller is the $g^{(2)}(0)$, the smaller is the probability to have more than one photon emitted at each time.

In our case if we have $g^{(2)}(0) < 0.5$, it means that we have a single photon emitter.

1.3 Solid-state single photon emitters characteristics

Solid-state SPE is an object of nanometric size made by semiconductor (SC) materials or that presents a semiconductor-like band diagram.

Different mechanisms can be present in a solid-state SPE that allow only a single photon to be emitted at each time. The most important of them for colloidal QDs is probably the Auger effect.

1.3.1 Non radiative recombination

A non-radiative recombination allows the annihilation of an exciton[2] without the emission of photons. The most important processes among them are :

- Auger recombination ;
- Exciton-phonon interaction ;
- Charge trapping.

1) Auger recombination

As we can see in figure 1.2, an exciton recombines (on a SC or colloidal QDs) giving to a carrier in the valence band (VB) its energy.

The excited carrier stays in the conduction band (CB) at a higher-level state without being ionized.

Thus, the carrier can relax non radiatively to the ground state of the CB.

Finally, when there is one exciton on the CB, it relaxes radiatively with the emission of one photon.

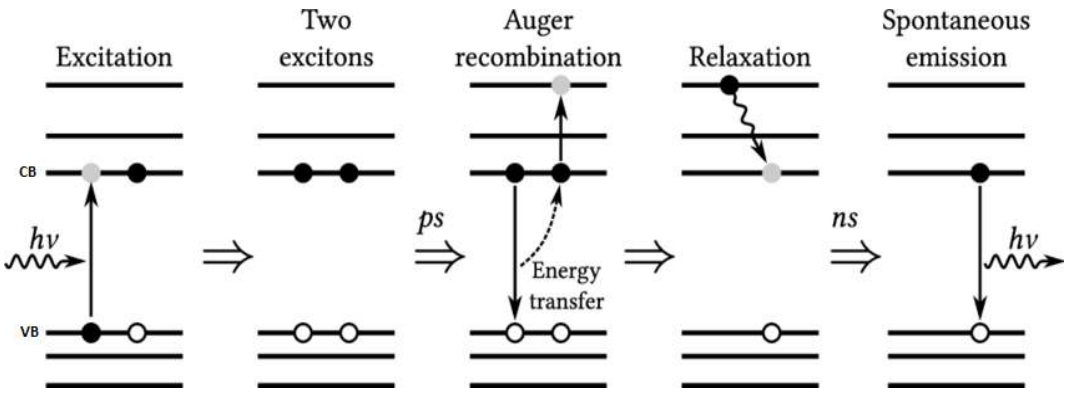

Figure 1.2: Auger recombination diagram [17]. CB : Conduction band & VB : Valence band

Remark : The Auger recombination is usually a very efficient mechanism due to the fact that until the Auger recombination is possible, it is predominant on the radiative recombination.

2) Exciton-phonon interaction

We distinguish two different cases :

- Intraband relaxation : Fast process, order of 100 fs [37] in which emission happens at the lowest energy and we can see one emission peak ;
- Interband relaxation: Spectrum broadening and creation of a non-radiative relaxation channel.

[2]Neutral quasi-particle, formed by the bounding of an electron and hole corresponding to an elementary excitation

3) Charge trapping

Carriers can be trapped onto a defect of the lattice or at the surface on the NC.

A trapped state can least from tens of picoseconds up to several seconds and its desexitation is usually non-radiative.

1.3.2 Blinking & bleaching

Emitter's quantum efficiency can be determined by different phenomena such as blinking and photobleaching [23].

1) Blinking

From what is reported in Park *et al.* (2015) [25], the blinking is the intermittency of the luminescence intensity between a dark/gray and a bright state when charges are trapped. In other words, it consists in strong fluctuations in the PL of a single emitter under excitation : the emitter's PL switches from "on" to "off" states (i.e from bright to dark/gray states, respectively) on time scales spanning from microseconds to hundreds of seconds.

Different analysis can be performed on blinking NCs [10] but here the most important one on which we will focus is the binning analysis.

Binning analysis :

We can perform a time correlated single photon measurement if photons arrive using a single photon detector.

Thus, plotting a histogram giving the number of photon with respect to their arrival times, we can analyse the distribution of the "on/off" states.

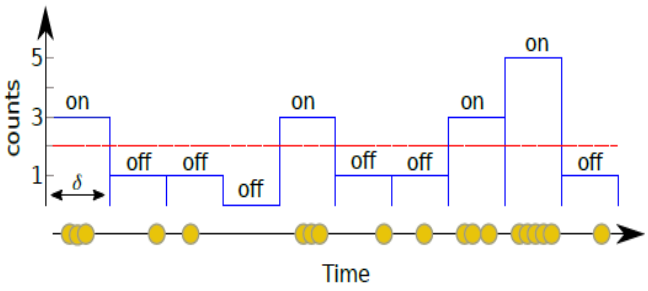

Figure 1.3: Blinking trace example. Each bin of the histogram reports the number of photons (in yellow) arrived at the time delay δ. A threshold is then chosen and the bin over the threshold is considered as an "on" state while the bin under it, is considered as an "off" state [26]

More generally, different kinds of blinking correspond to different relaxation mechanisms.

It has been shown that we can distinguish two types of blinking :

- Type A : The "on" to "off" switch happens when a carrier is moved to a trap state : this trapping usually happens with thermal ionization or Auger-assisted

photo-ionization. The opposite process, "off" to "on" switch, happens when the carrier is released, typically with a relaxation process ;

- Type B : The intensity fluctuation is due to a fast trapping of high energy electrons followed by a non-radiative recombination of the electron and the hole.

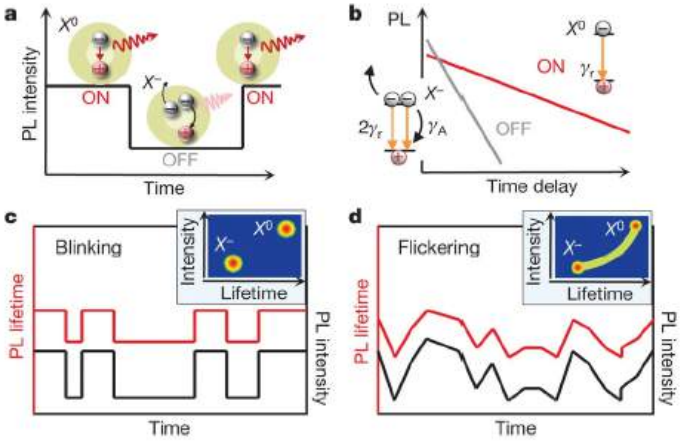

Figure 1.4: Type A blinking mechanism : (a) "On" periods : neutral state & "off" periods : negative charge excitation state; (b) PL decay of the "on/off" states on a logarithmic scale; (c) Blinking behaviour between two separated states corresponding to two different spots in the fluorescence lifetime intensity distribution (FLID) image & (d) Flickering behaviour corresponding to a visible curve in the FLID image, source : Galland *et al.* (2011) [10]

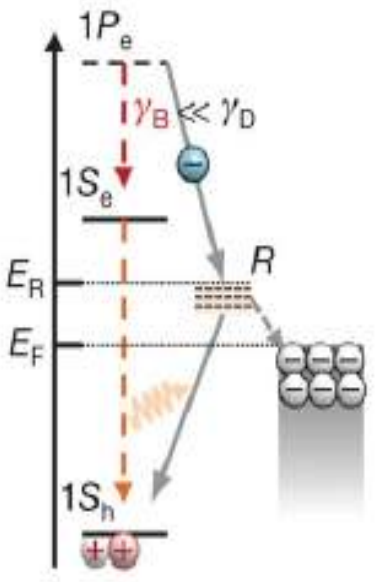

Figure 1.5: Type B blinking mechanism : "Off" periods due to the activation of recombination centres (R) that capture hot electrons at a rate $\gamma_D \gg \gamma_B$: intraband radiative rate (the ground and the excited electron states are shown as $1S_e$ and $1P_e$ respectively; $1S_h$ is the band-edge hole state), source : Galland *et al.* (2011) [10]

Remarks :

➢ In order to have a good signal/noise (S/N) ratio, we can't choose a small bin size ;

➢ We cannot define a finite temporal resolution for the detector.

2) Bleaching

The photobleaching phenomenon caused by an irreversible process imply an efficiency drop.

Bleaching often takes place at longer time scales than blinking.

Finally, we conclude this section adding the fact that for a single photon source, we must suppress or reduce blinking and bleaching phenomena.

1.3.3 Hanbury-Brown & Twiss interferometer

The second-order autocorrelation function was conceptually introduced by the experimental work of Hanbury-Brown and Twiss in 1950, when they developed an intensity interferometer to measure the angular diameter of stars [4].

As we can see in figure 1.6 a), a stream of photons arrive incidentally on a 50:50 beam splitter that equally divides it between the two outputs on the detectors D1 and D2. The resulting output beams are fed into an electronic unit ("counter/timer") which counts the number of pulses from each detector and records the time elapsed between counts from D1 and D2 (see figure 1.6 b)).

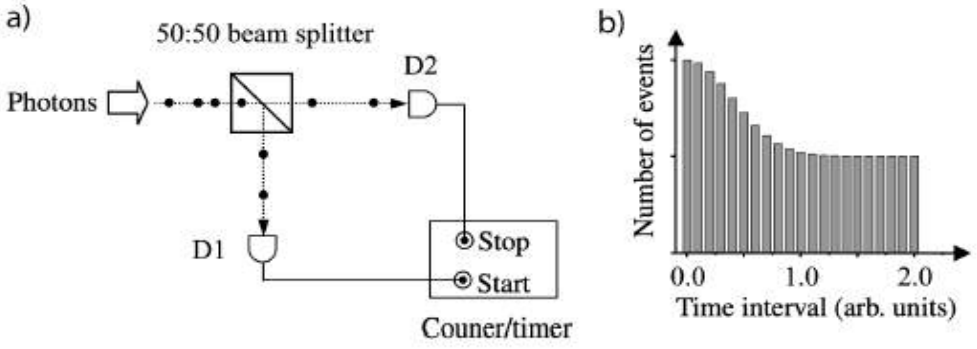

Figure 1.6: a) Hanbury-Brown and Twiss (HBT) experiment b) Histogram showing the number of events recorded in a particular time interval for a bunched photon stream [9]

Knowing that the number of counts on a photon-counting detector is proportional to the intensity, the second-order autocorrelation function defined by :

$$g^{(2)}(\tau) = \frac{\langle I(t)I(t+\tau)\rangle}{\langle I(t)\rangle^2}$$

Can be written as :

$$g^{(2)}(\tau) = \frac{\langle n_1(t)n_2(t+\tau)\rangle}{\langle n_1(t)\rangle \langle n_2(t+\tau)\rangle} \tag{1.11}$$

Where $n_1(t)$ and $n_2(t)$ are respectively the number of counts on detectors D1 and D2 at time t. As already mentioned previously, this quantity gives the conditional probability of detecting a second photon at time $t + \tau$, given the detection of a photon at time t. By varying the time delay between the detection events, $g^{(2)}(\tau)$ can be measured.

Chapter 2

Perovskite nanocrystals

2.1 Chemical composition & crystallographic structure

A perovskite is a material with a crystal structure like the mineral called perovskite, which consists of calcium titanium oxide ($CaTiO_3$) [39].

The general chemical formula for perovskite compounds is ABX_3, where A (organic/inorganic) and B (metal) are two cations, often of different sizes, and X (halide) is an anion that bonds to both cations. The A atoms are generally larger than the B atoms. This mineral had the peculiarity, to present a particular cubic structure.

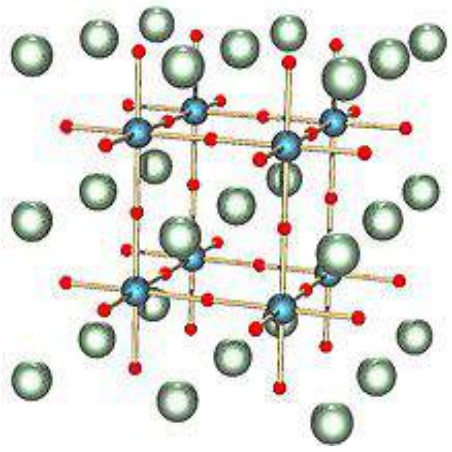

Figure 2.1: ABX_3 perovskite undistorted cubic structure. The red spheres are X atoms, the blue spheres are B atoms, and the green spheres are the A, source : *Wikimedia Commons*

Furthermore, perovskites undergo structural changes upon application of external stimuli, such as temperature, pressure or applied electric field [3]. However, perovskite NCs such as $CsPbBr_3$ can behave as very efficient SPEs. Their emission wavelength can be tuned, playing on their size and composition, together with their coherent emission [36].

Using them, we can obtain single photon emission at low [30] [15] and room [25]

temperatures.

Thus, as one of the most abundant structural families, the interest in perovskites, originally studied for solar-cell applications [24], has increased in the quantum optics community knowing that they are promising nano-objects for quantum applications [2]. Moreover, they are easily synthesized by low-cost, well-mastered wet-chemistry techniques.

Despite these facts, the main problem to tackle in this context is their photostability under optical excitation.

2.2 Electronic & optical properties

2.2.1 Band structure in perovskite nanocrystals

All $CsPbX_3$ ($X = Cl$, Br, I) perovskites compounds have similar electronic properties and are characterized by a direct tuneable band gap [19] at the R point of the band structure (see figure 2.2).

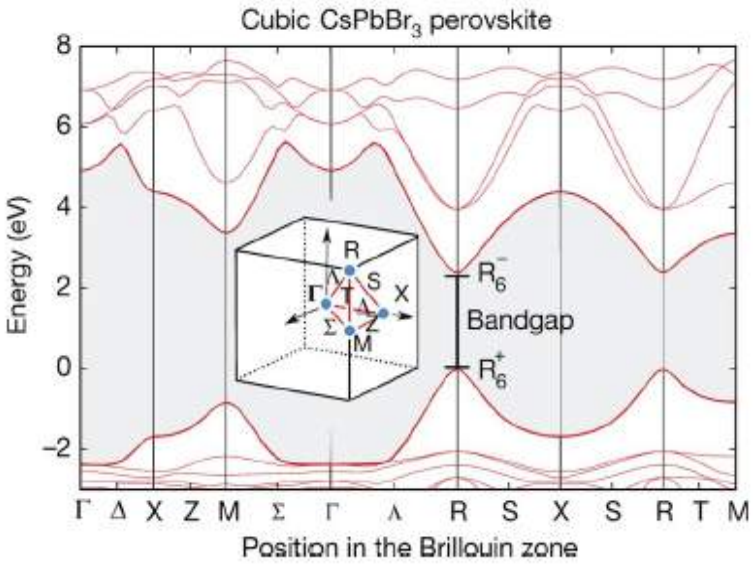

Figure 2.2: Band structure of $CsPbBr_3$ perovskite with a band gap of 2.23 eV [33] (T = 300 K) [1]. Inset : First Brillouin zone of a cubic crystal lattice

Furthermore, their PL is characterized by high QYs of 50-90 % and narrow linewidths[1] of 12-45 nm. Moreover, in order to investigate the size-dependent fluorescent colors of $CsPbX_3$ perovskites, several attempts to reduce the perovskites bulk size to the sub-micron scale have been performed [35] [6], until the synthesis of NCs of sizes close to the exciton Bohr radius, corresponding to 7 nm in the case of $CsPbBr_3$ [29]. Reducing the dimension of these NCs, significantly changes their electronic energy spectrum, resulting in a transition from continuous to discrete energy levels and thus reaching the quantum-confined regime [13].

[1]Full width at half maximum (FWHM)

This achievement allowed to explore their quantum properties [12], demonstrating an antibunching behaviour of their PL emission [25].

N.B : For more information about the electronic and optical properties, see the references [22] [40].

2.2.2 Perovskite nanocrystals as single photon emitters

1) Photobleaching properties of perovskite nanocrystals

Perovskites NCs emitters like other kinds of QDs do bleach. They are degraded by moisture and light as they have a higher surface/volume (S/V) ratio.

It has been observed, looking at the spectrum of the emitted light, that by exciting perovskite NCs, their structure progressively degrades, starting from the external layers.

This is due to the fact that, during the measurement, the emission light spectrum is blue shifted i.e crystals progressively become smaller with a decrease of the emission wavelength (see figure 2.3). At the end, the emitters become completely dark (i.e they bleached).

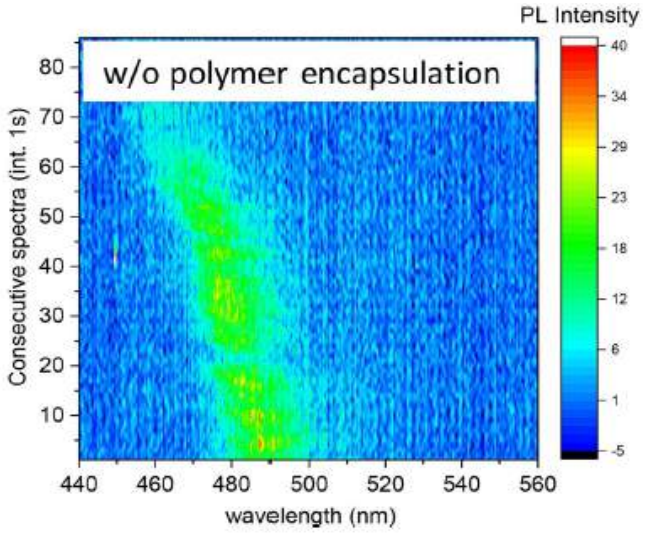

Figure 2.3: Blue shift of the emission wavelength of single perovskite NC. The green trace shows the evolution of the emitted signal during time, source : Rainò *et al.* (2019) [31]

2) Photon antibunching of pervoskite nanocrystals

Single photon emission from perovskite NCs has been reported firstly by Park *et al.* in 2015 [25] with an experiment at room temperature. They describe single photon emission from perovskite nanocubes made of $CsPbBr_3$, $CsPbI_3$ and $CsPbBr_xI_{(3-x)}$.

The emission spectra reported in figure 2.4 (a) shows us that changing the composition of the perovskites, we can modify the emission wavelength, whereas in figure 2.4 (b), we can see that the autocorrelation function $g^{(2)}(0) = 0.05$ of the emitted light is very low and thus these NCs are very good SPEs.

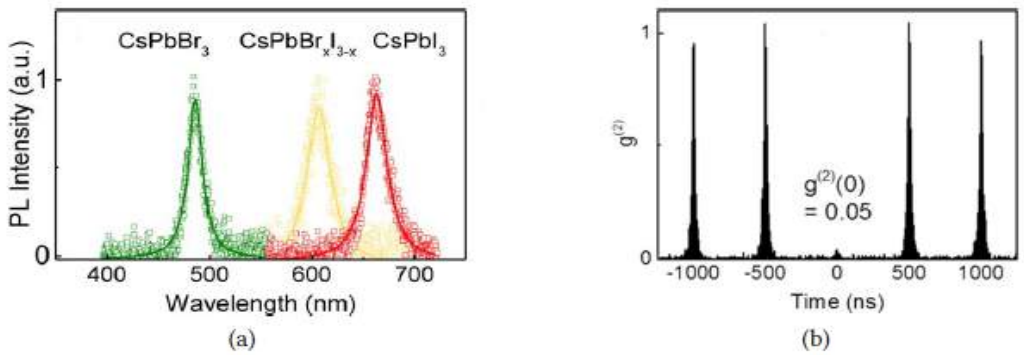

Figure 2.4: (a) Different emission spectra with different composition of perovskite NCs (b) $g^{(2)}(\tau)$ measurement of light emitted from a single perovskite NC, excited with a pulsed laser [25]

Chapter 3

Experimental setup & methods

3.1 Perovskite nanocube fabrication

In order to characterize $CsZnPbBr_3$ doped and $CsZnPbBr_3 - PEI$ perovskite NCs, samples were initially prepared by Emmanuel LHUILLIER at the INSP with a concentration that depends on the type of measurement to be made.

As our final purpose is to couple a single emitter to a tapered optical nanofiber to develop an integrated single photon source, we need to use a strongly diluted sample. It is then crucial to investigate the behaviour of the emitters as a function of the concentration.

In order to study the dilution effect on the perovskite NCs stability, we have to carry out a dilution using toluene as solvent. For this reason, we prepared five samples using different dilutions starting from the most concentrated colloidal solution (typically with a molar concentration between 1 μM-2 μM), up to a dilution of 1:50 and above (1:500).

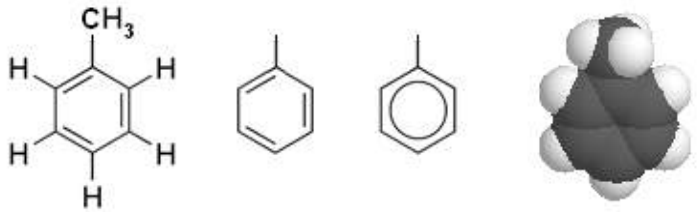

Figure 3.1: Representations of toluene (semi-developed, 3D), source : *Wikipedia Commons*

For each concentration, we deposited over glass coverslips (BK7, 180 nm thick), a droplet of 20-30 μL of the colloidal solution with a pipette and used the spin-coating, spreading homogeneously the thin film of the colloidal solution over the coverslips due to centrifugal force. As there is a uniform evaporation of toluene (high volatile component) due to the fast rotation of the spin-coater, it is removed from the coverslips and only the NCs remain on their surfaces.

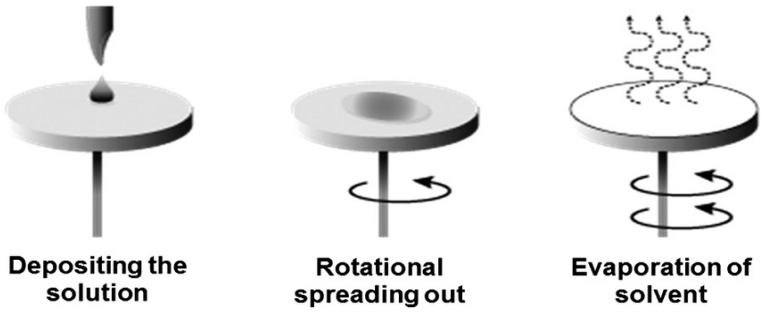

Figure 3.2: Spin-coating processes, source : G. Amokrane *et al. ScienceDirect,* 2018

We started by analysing the highest concentration sample making sure that we can individually target each emitter so that we could conduct a study on the individual emitter.

Finally, we store the samples protected from light and moisture at room temperature.

3.2 Fluorescence microscopy

We optically characterized the NCs using an inverted confocal microscope and performing all the measurements at room temperature.

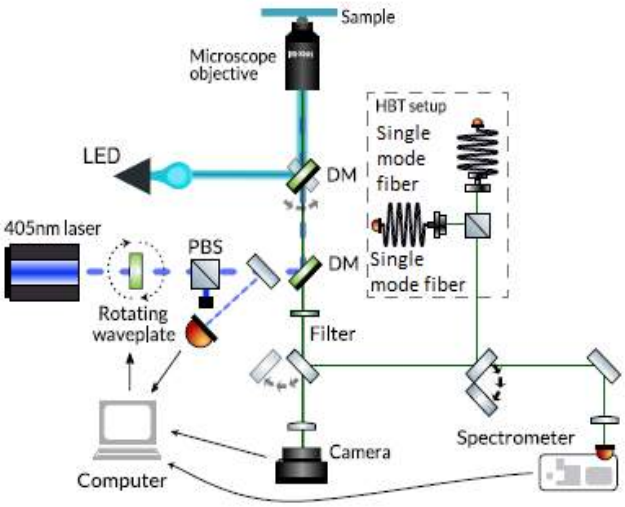

Figure 3.3: Inverted confocal microscope setup for the sample analysis. DM : dichroic mirror. PBS : polarizing beam splitter, source : Pierini *et al.* (2020) [27]

First of all, in this setup, the coverslips containing the samples are mounted on a motorized stage (MadCityLabs) fixed on the inverted microscope (Nikon Eclipse Ti). This stage allows an (xy) plane displacement such that the whole sample can be investigated.

Furthermore, to obtain an increase of the collection of photons, it is useful to use an oil immersion objective, in which a small drop of oil is deposited between the front lens of the objective and the glass coverslip. In our measurements, we used

an oil objective with a numerical aperture NA = 1.4, a magnification of 100 × for standard fluorescence and antibunching measurements.

Thus, the emitters can be excited with a LED or a pulsed laser (see figure 3.3) depending on the measure that we wanted to do. The emission can be detected on a camera or analyzed with a spectrometer.

Finally, we can perform a $g^{(2)}$ measurement with a HBT setup, with single mode optical fibers connected to avalanche photodiodes (APDs).

3.2.1 Wide-field setup

Following the steps mentioned above, a non-collimated light-emitting diode (LED) lamp at 400 nm is reflected by the first dichroic mirror (DM1, EDMUND) with a cut-off at 432 nm and placed at an incident angle of 45° from the incoming LED light which is focused by the objective lens to the sample (see figure 3.4a). After filtering out the excitation with a 430 nm long-pass filter, the luminescence of perovskite nanocubes collected by the objective lens can be sent to the high quantum-efficiency CCD camera (HAMAMATSU ORCA Flash 4.0 LT) in order to locate the emitters, collect an image of the field of view of the microscope (see figure 3.4b) and study perovskite NCs photostability under illumination.

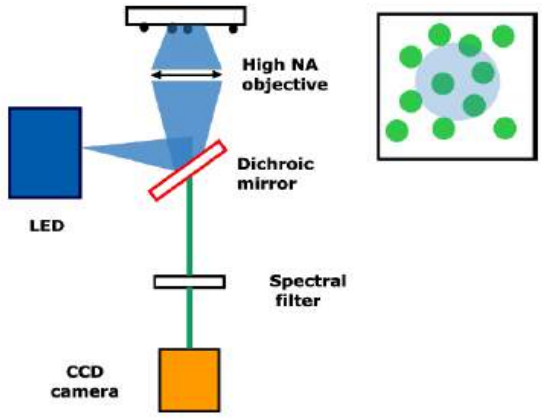

(a) Wide-field configuration setup [5]

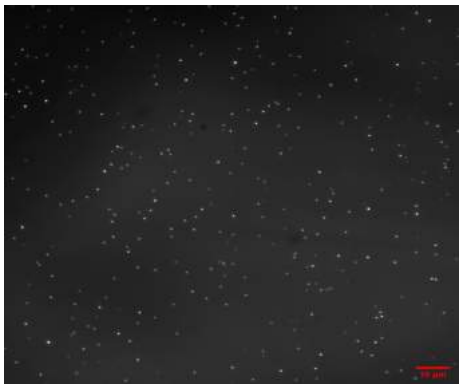

(b) Multiple emitters on the diluted (1:200) $CsZnPbBr_3$ doped perovskite NCs sample (emitters are the bright spots on the dark background)

Figure 3.4: Wide-field setup & overall emitters image

3.2.2 Confocal microscopy setup

The confocal microscopy is fundamental for isolating and detecting single emitters without exciting simultaneously several emitters and collecting the light emitted from the neighbours.

To study the fluorescence from different single NCs over a large area on the substrate, the sample is scanned using the motorized stage previously mentioned. This stage allows displacements with an accuracy of less than 1 μm, a repeatability of less than 100 nm, a step resolution of 95 nm and a maximum speed of 2 $mm.s^{-1}$. The stage is positioned such that the single NC is at the center of the laser spot.

Once the single emitter position is identified, we excite it with a 405 nm picosecond pulsed laser (pulse width < 50 ps), reflected by the second dichroic mirror (DM2, SEMROCK) placed at an incident angle of 45° from the incoming laser light which is focused by the objective lens to the sample, with a repetition rate of 2.5 MHz (see figure 3.5a).

After filtering out the excitation with a 430 nm long-pass filter, the collected light can be imaged on the high quantum efficiency CCD camera (see figure 3.5b) or collimated by a lens and sent to a spectrometer equipped with a similar high quantum-efficiency CCD camera to verify the emitter stability taking a PL spectrum, checking the presence of a single narrow peak (meaning that we don't have a cluster of emitters), then carrying a saturation measurement to determine the saturation intensity or even using a flip mirror, sent to a pair of avalanche photodiodes (APDs, EXCELITAS) in a Hanbury-Brown and Twiss (HBT) configuration. In this last case a 50:50 beam splitter divides the PL in two arms and the PL is focused by means of two lenses on the respective detectors.

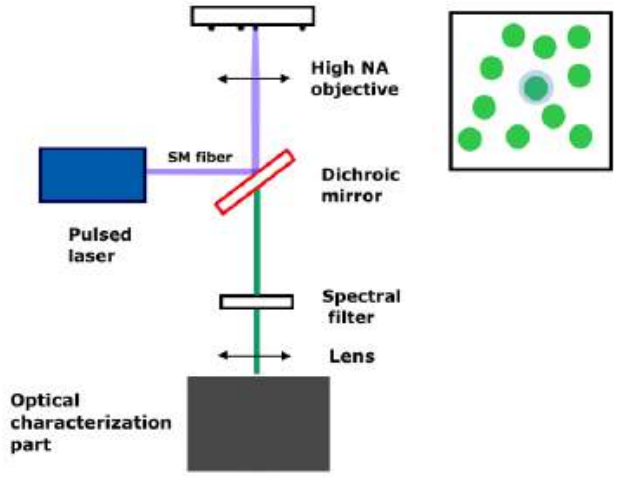

(a) Confocal microscopy configuration setup. SM fiber : Single-mode fiber [5]

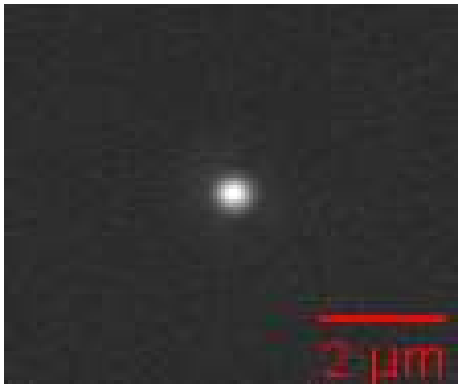

(b) Single emitter on the diluted (1:200) $CsZnPbBr_3$ doped perovskite NCs sample (emitter is the bright spot on the dark background)

Figure 3.5: Confocal microscopy setup & single emitter image

3.3 Photobleaching

As we know, several studies presented lead halide perovskites NCs emission instability [14].

Here below are the two main analysis of photobleaching :

- Blue shift of the emission wavelength : In that type of characterization, each sample is strongly illuminated with light from the laser while the spectrum of the sample is recorded. Analysing each spectrum (taking one spectrum every minute for one hour), we can estimate the blue shift of NCs emission wavelength ;

- Robustness of NCs : In that type of characterization, each sample is strongly illuminated with light from the LED lamp (full irradiance 25 W) while a video of the sample emission is recorded. Analysing each frame of the video (taking one picture[1] every minute for one hour), we can estimate the number of NCs that are still emitting from the first frame.

3.4 Photon antibunching

To characterize the quantum emission and verify if our NCs can be used as SPEs, we measured the autocorrelation function $g^{(2)}(0)$ using a Hanbury-Brown and Twiss (HBT) setup (grey dashed line setup in figure 3.6).

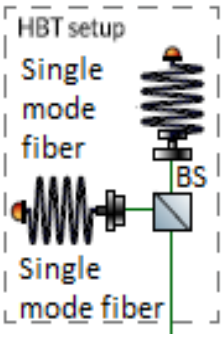

Figure 3.6: HBT setup. BS : Beam splitter, source : Pierini *et al.* (2020) [27]

As we have already mentioned on section 1.3.3, experimentally the beam is divided in two parts by a 50:50 beam splitter and even if to perform correct measurements of $g^{(2)}(0)$, we can use a photon-resolved single photon detector, here the two beams are sent to two different avalanche-photodiodes (APDs) through single mode fibers. We record the arrival times with the time tagged time-resolved (TTTR) method [38] (Picoquant PicoHarp 300 TCSPC card used, together with a Picoquant PHR 800 router) using the TCSPC technique (see section 3.4.1 below).

Finally, we create a histogram of the relative arrival times of the photons with a time bin. The histogram is thus normalized by setting the mean height of the peaks. This procedure is well-established and documented in the literature [32] [21].

3.4.1 Time-correlated single photon counting

We use a time-correlated single photon counting (TCSPC) system to efficiently measure the arrival times of fluorescence photons. In our case, as mentionned above, the electronic system consists of a PicoHarp 300 acquisition card together with the PHR 800 4-channel detector router form PicoQuant.

The measurements that we carried out with this technique allow us to derive several quantities of interest : the correlation function of the signal at short time delays, the PL decay and the PL as a function of time.

[1] 1 picture = 3 frames

1) Correlation function

By measuring the temporal correlation between the events given by the detection of a photon, we can reconstruct the second-order autocorrelation function of the typical intensity of the emitter.

Once the first photon is detected, the APD generates a pulse which is sent to the electronics.

Thus, a histogram of the number of "start-stop" coincidences with respect to the time interval between detection events is build, dividing the entire range of time values into series of intervals of a certain temporal width, called bin time, and counting the number of events detected during a given **bin time.** This histogram reproduces, at small delays, the second-order autocorrelation function $g^{(2)}(\tau)$ of the intensity. If the autocorrelation function displays an antibunching behaviour, we know that we are studying a single emitter.

Remark : To correlate each photon arrival time with the next one, we need to use the HBT configuration, knowing that we cannot evaluate the photon statistics of a quantum state of light with only one detector.

2) PL decay & trace

In this case, a synchronization signal (SYNC) is set on the laser, used as a reference (see figure 3.7).

Thus, the excitation laser triggers a timer, which is stopped with the detection of a fluorescence photon. This time delay between the excitation of the NC and the emission of a photon is called **microtime t.**

Furthermore, for each pulse, the absolute arrival time with respect to the beginning of the experiment is recorded. This time between the beginning of two pulses is called **macrotime T.**

Each recorded pulse is labelled with a specific **microtime t** and **macrotime T** with the pulse generated APD channel.

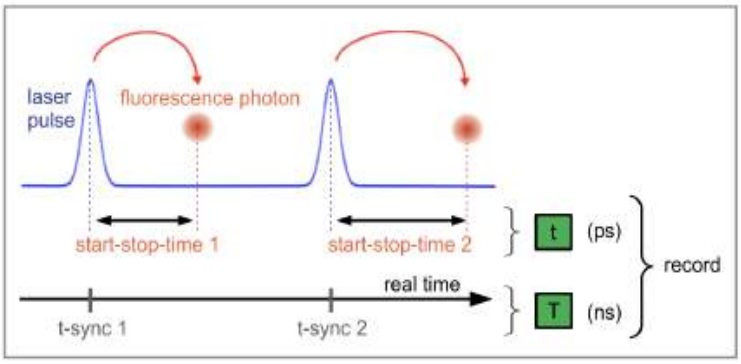

Figure 3.7: Scheme of the PL data acquisition, source : *PicoQuant*

Finally, we get the PL decay by plotting the histogram of the **microtime,** with a bin width being a multiple of the resolution (e.g 512 ps) whereas the PL trace [2] by plotting the histogram of the **macrotime** counting the number of photons detected

[2]PL trace = Intensity (counts/10ms) as a function of time

during a given bin time (this bin time should be both short and long in order to observe fast intensity fluctuations and avoid noise, respectively, e.g 50 ms).

Remark : As we have different background sources of noise in our set-up, such as room light, reflected excitation light and dark counts of the APDs, they affect the $g^{(2)}$ value that we get from TCSPC measurements. For that reason, it is necessary to clean the $g^{(2)}$ histogram from them. The method used here to correctly perform the $g^{(2)}$ measurement is explained in Annex A.

Chapter 4

Results & analysis

4.1 Perovskite emission spectra

A typical emission spectrum of the $CsZnPbBr_3$ doped and the $CsZnPbBr_3 - PEI$ single NCs are shown in figure 4.1.

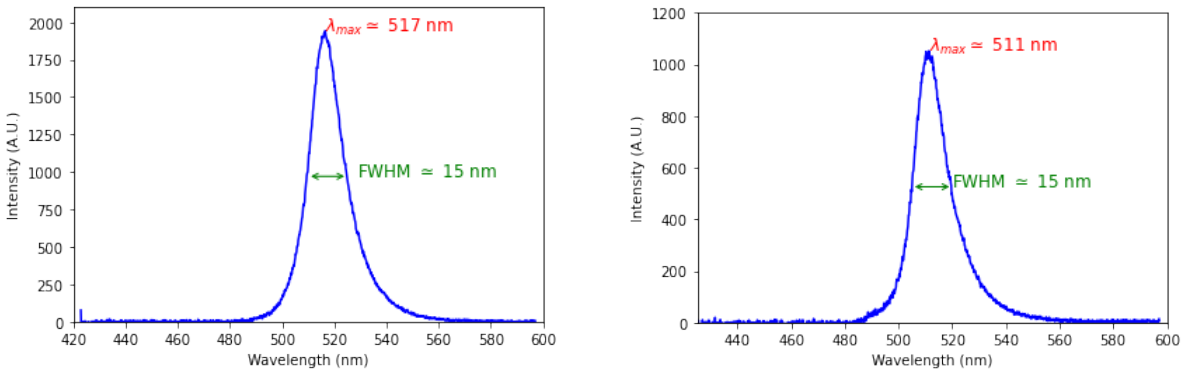

(a) $CsZnPbBr_3$ doped single NC spectrum

(b) $CsZnPbBr_3 - PEI$ single NC spectrum

Figure 4.1: Typical emission spectra of single perovskite NCs

They are characterized by a wavelength of 517 nm and 511 nm respectively with a FWHM for both perovskites of about 14-15 nm.

These associated emission wavelength shows us that comparing with the work carried by Kovalenko *et al.* (2017), where the perovskite emission wavelength was about 520 nm and the mean FWHM about 20 nm for the bulk perovskite [18], that in our case, we have a confined emission.

4.2 Saturation measurement

The saturation is a typical effect in deterministic SPEs regarding the emitted intensity that says that at a certain point, due to the Auger recombination, exciting the perovskite NCs with a higher intensity would not imply a higher emission number of photons.

In our case of not-so-efficient Auger effect, the emitted intensity as a function of the excitation intensity is described by the below equation :

$$P_{PL}(I) = P_{sat}(1 - e^{-\frac{I}{I_{sat}}}) + BI \tag{4.1}$$

The first term of the sum represents the saturating part that is due to the single exciton component whereas the second term is due to the biexciton[1] emission.

For each emitter that we studied in the case of $CsZnPbBr_3 - PEI$ perovskites, we measured the emitted intensity as a function of the excitation power, subtracting the background from the experimental data.

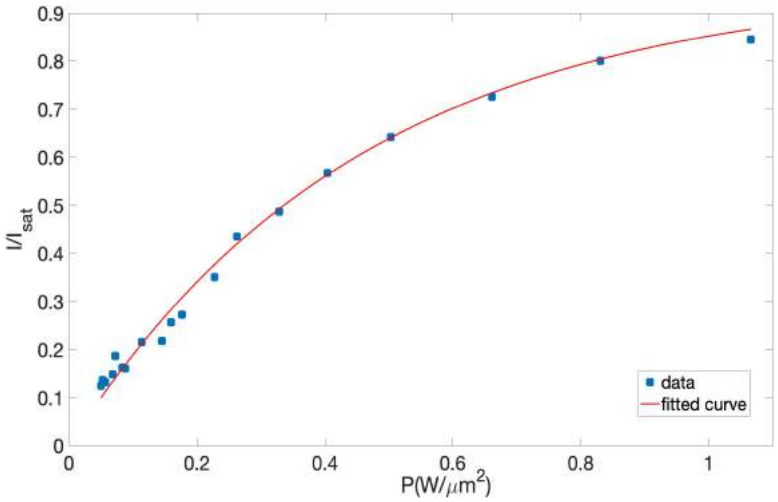

Figure 4.2: Example of a saturation measurement of a single NC (P_{sat} = 50 nW) : The blue dots are the experimental data while the red curve is the fitted function from equation 4.1

We observed a saturation value P_{sat} of 50 nW which will be the reference for the different emitter's characterization. But, this saturation curve must be completed with more experimental values, in order to conclude on the presence or not of multiexcitons.

[1]Biexciton : In condensed matter physics, biexcitons are created from two free excitons

4.3 Photobleaching characterization

4.3.1 Blue shift of the emission wavelength

As we have already mentioned, the emission instability of perovskite NCs is a critical challenge and the subject of several research [14]. One way to study the photostability of the NCs is to see their emission wavelength shift behaviour as a function of time.

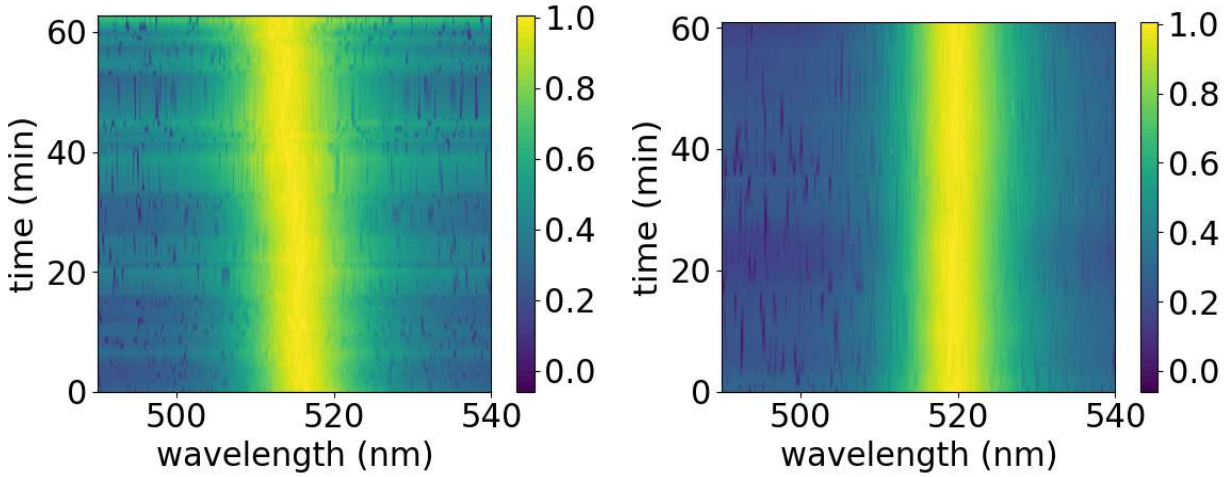

(a) $CsZnPbBr_3$ doped single NC blue shift

(b) $CsZnPbBr_3 - PEI$ single NC blue shift

Figure 4.3: Normalized evolution of the emission wavelength at saturation intensity. The normalization is set to the maximum intensity

A blue shift of the emission wavelength about 4-5 nm after one hour is observed in the case of the $CsZnPbBr_3$ doped NCs whereas there is no blue shift in the case of the $CsZnPbBr_3 - PEI$ NCs. The observed spectral drift in the case of the $CsZnPbBr_3$ doped NCs is attributed, to the degradation of the NCs, resulting in a reduction of their sizes.

In other words, we obtain a photostability improvement using our $CsZnPbBr_3 - PEI$ NCs but also the $CsZnPbBr_3$ doped NCs under illumination with strongly reduced bleaching effects compare to the previous works present in literature.

4.3.2 Robustness of nanocrystals

The other way to study the photostability of perovskite NCs is to count the number of NCs as a function of time which qualify the robustness of the NCs.

Moreover, as we wanted to couple single emitters to a tapered optical nanofiber, we also studied the emitters stability behaviour varying the concentration of our $CsZnPbBr_3$ doped and $CsZnPbBr_3 - PEI$[2] using the approach of Raino *et al.*

[2]Perovskite emitters with a polymer is not the best suitable option for photonic applications that need single nano-objects to be precisely positioned as the presence of polymer, takes place, perturbing the near field

(2019) with colloidal solutions [31], in order to see in this latest case, if there is a particular effect adding PEI to the $CsZnPbBr_3$ doped NCs.

Finally, the measurements were taken using the photobleaching setup of the NCs robustness characterization (see section 3.3).

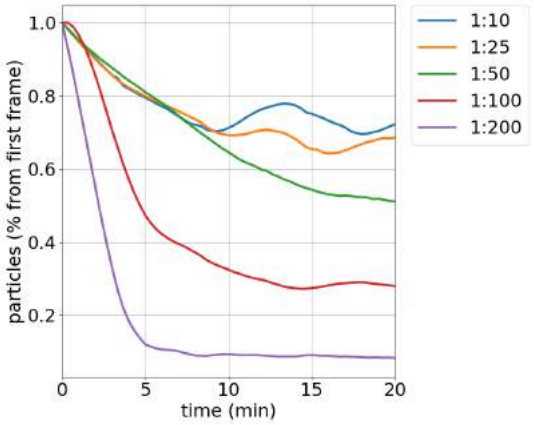

(a) $CsZnPbBr_3$ NCs robustness

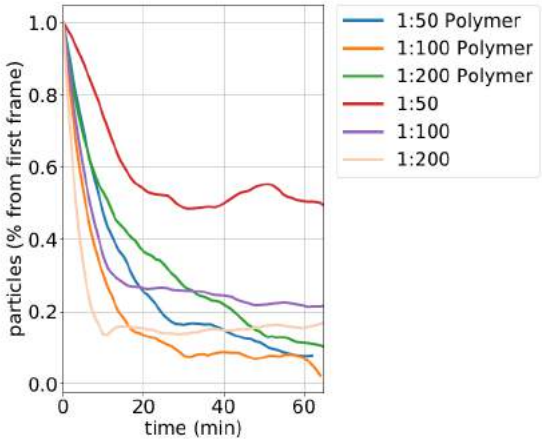

(b) $CsZnPbBr_3 - PEI$ NCs robustness

Figure 4.4: Perovskite NCs emitting after a certain time under strong illumination with respect to the initial solution dilution (1:X means X times diluted)

Comparing, with the results present in the literature, we can clearly see that in the case of $CsZnPbBr_3$ doped NCs, both the low diluted sample (1:10 solution) and the high diluted samples (dilutions from 1:25 to 1:200) have a high photostability with more than half of the emitters still working after 10 min (and even more) for dilutions 1:10 to 1:50 (see figure 4.4 (a)).

Now, if we compare, the percentage of NCs emitting after a certain time under strong illumination as a function of the time between $CsZnPbBr_3$ doped NCs and $CsZnPbBr_3 - PEI$ NCs, we can see that for the same dilution ratio we can't compare the robustness between these two NCs samples with respect to time due to the fact that it is more appropriate to study it for the same concentration (i.e same number of NCs on the same fixed volume in μm^2) between both samples.

Finally, we can conclude this section that we generally see that the dilution process leads to poorly passivated NCs which can easily bleach.

4.4 Emission lifetime

As we discuss in section 1.3.2, the emitted intensity of a NC is not constant in time but tends to fluctuate : phenomenon known as blinking.

A well-established method to experimentally distinguish between Type A and Type B blinking is to study the spontaneous emission lifetime dependence on the emission intensity.

Even if we don't study this case, here we will just present the lifetime behaviour of the $CsZnPbBr_3 - PEI$ perovskite NCs.

The measure of the decay rate associated to the emission through lifetime measurement corresponding to the spontaneous emission of the emitter is defined by :

$$\tau_r = \frac{1}{\gamma_r} \tag{4.2}$$

With γ_r : the radiative decay rate and τ_r : the emission lifetime.

It can be measured using a TCSPC measurement.

If multiple emission states are present, multiple lifetimes are measured and are defined as :

$$I = \sum_i A_i e^{-\frac{t}{\tau_i}} \tag{4.3}$$

With i : the radiative states.

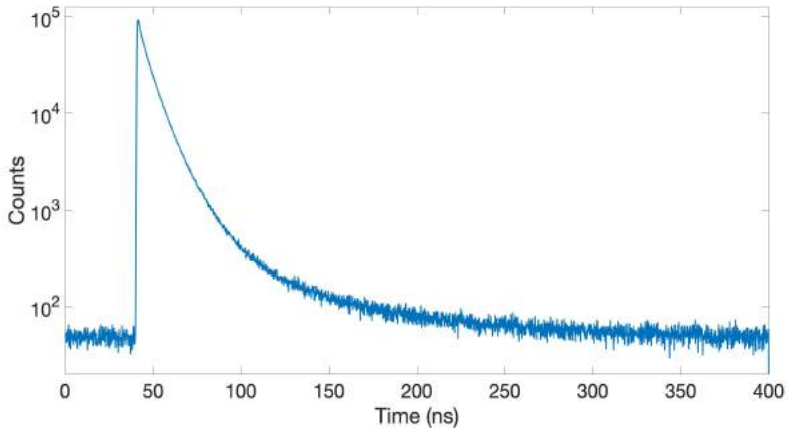

Figure 4.5: Example of a $CsZnPbBr_3 - PEI$ single NC lifetime decay without fit

To perform more quantitative analysis, we fit the lifetime histogram of our $CsZnPbBr_3 - PEI$ with a triple-exponential decay model :

$$A_1 e^{-\frac{t-t_0}{\tau_1}} + A_2 e^{-\frac{t-t_0}{\tau_2}} + A_3 e^{-\frac{t-t_0}{\tau_3}} + B \tag{4.4}$$

With three different lifetimes, τ_1, τ_2, and τ_3, corresponding to neutral, charged, and biexciton state emission, respectively. t_0 represents the pulse arrival time, while A_i, $i \in \mathbb{N}^*$ are the amplitudes of each decay component and B is an offset added to consider the dark counts.

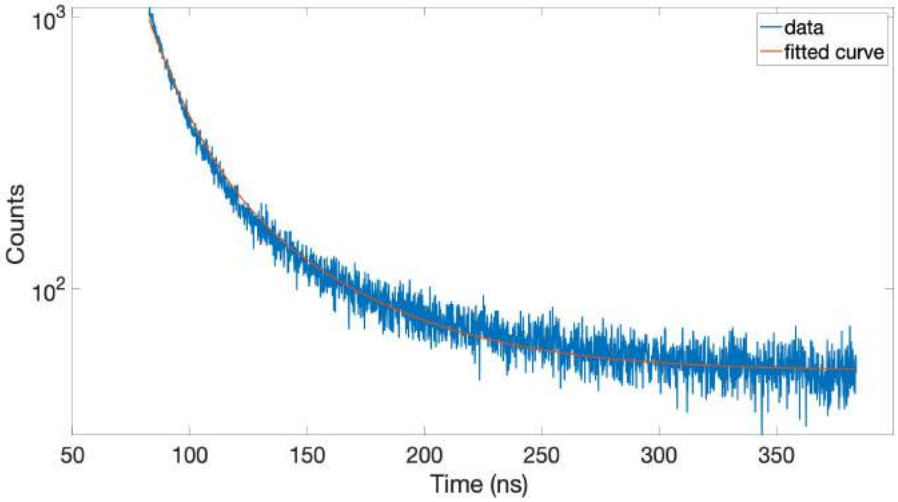

Figure 4.6: Example of a $CsZnPbBr_3 - PEI$ single NC lifetime, fitted with a triple exponential decay model

We observe that the experimental data satisfy the fitting and obtain 4 ns, 20 ns, and 40 ns for the lifetimes of the neutral, charged and biexciton emission states, respectively.

4.5 $g^{(2)}$ measurement

For each $CsZnPbBr_3 - PEI$ emitter, we measured the second-order autocorrelation function $g^{(2)}(0)$ using the Hanbury-Brown and Twiss setup and recording the data with the TTTR method using the TCSPC technique previously mentioned.

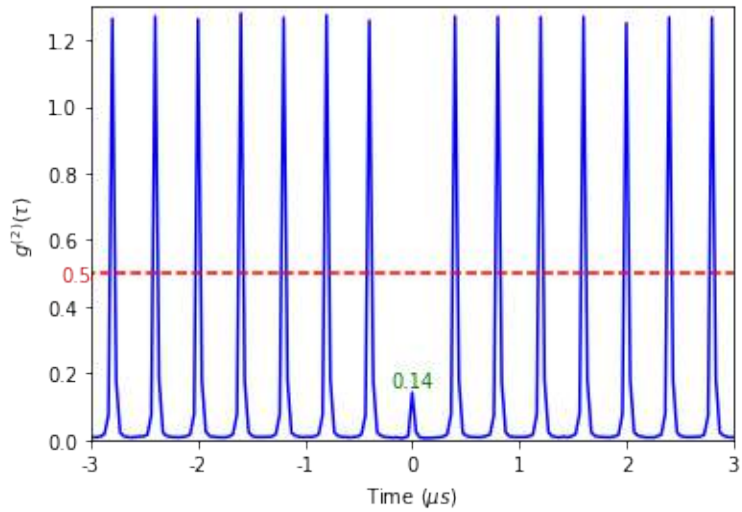

Figure 4.7: Example of $g^{(2)}(\tau)$ function of a single $CsZnPbBr_3 - PEI$ perovskite NC emitting high single photons, measured with a repetition rate of 2.5 MHz

The autocorrelation function peaks close to the 0 delay peak are higher than 1 which is due to the blinking.

Furthermore, a value of $g^{(2)}(\tau = 0) = 0.14$ delay is obtained at saturation intensity.

We can conclude that this value being well below 0.5 shows experimentally the clear signature of a single photon emission.

Chapter 5

Outlook & perspectives

In this Master 1 internship report, we presented the optical and quantum properties of highly photostable $CsZnPbBr_3$ doped and $CsZnPbBr_3 - PEI$ perovskite NCs.

Perovskite NCs have shown to be high quality emitters, with a narrow peak emission at room temperature and easy fabrication method. But their photostability is the main problem. In recent years there has been a development of the synthesis method of $CsPbBr_3$ perovskites in order to tackle this issue.

The study of Pierini *et al.* (2020) using $CsPbBr_3$ perovskite NCs [27], has shown that one of the factors is the role of the ligands which is not completely understood and the dilution of the studied pervoskite colloidal solution.

Thus, we have carried out the study of the $CsZnPbBr_3$ doped and $CsZnPbBr_3 - PEI$ perovskite NCs in order to have a better understanding of the ligands and dilution issues present in the literature.

We have seen that the $CsZnPbBr_3$ doped and $CsZnPbBr_3 - PEI$ perovskite NCs emitters exhibit a remarkable stability of about two orders of magnitude better than the previously reported results in literature.

Furthermore, we have studied the lifetime behaviour of the $CsZnPbBr_3 - PEI$ perovskite NCs.

Moreover, we have demonstrated the single photon behaviour in $CsZnPbBr_3 - PEI$ perovskite NCs.

Finally, further perspectives will be the study of the second-order autocorrelation function of $CsZnPbBr_3$ doped perovskite NCs, the robustness comparison for a same concentration and fixed volume of both $CsZnPbBr_3$ doped and $CsZnPbBr_3 - PEI$ perovskite NCs and then the coupling of a single $CsZnPbBr_3$ doped perovskite NCs with a high dilution ratio to a nanofiber carrying the same optical and quantum characterization studies in order to realize a compact, integrated, hybrid single photon devices at room temperature [7] [28] [27].

Appendix A

Noise cleaning on $g^{(2)}(\tau)$ measurements

To correctly perform the $g^{(2)}(\tau)$ measurement, we need to made some considerations on the coincidences counting method. We call $M(\tau)$ the number of counts measured at a given time delay τ.

Each count can be generated either by a start from the signal or from the background and by a stop from the signal or from the background.

Calling $s(\tau)$ the probability to have a start (or stop) generated by the signal and $b(\tau)$ the probability to have the start (or stop) generated by the background, we can write (when both $b(\tau)$ and $s(\tau) \ll 1$) :

$$M(\tau) = C(b(\tau) + s(\tau))(b(\tau) + s(\tau)) \tag{A.1}$$

Where C is a constant of proportionality.

We call $M' = \frac{M}{C}$. We consider τ_b in between two consecutive peaks, we know that there is no signal there and $s(\tau_b) = 0$.

$$M'(\tau_b) = b^2(\tau) \tag{A.2}$$

To find $M_c(\tau) = Cs^2(\tau)$, we solve the system given by equations A.1 and A.2 and we find that :

$$M_c(\tau) = M(\tau) + M(\tau_b) - 2\sqrt{M(\tau)}\sqrt{M(\tau_b)} \tag{A.3}$$

Using this formula, we obtained the $g^{(2)}(\tau)$ histogram cleaned from the background counts.

Bibliography

[1] Michael A. Becker et al. "Bright Triplet Excitons in Caesium Lead Halide Perovskites". In: *Nature* 553.7687 (11 Jan. 2018), pp. 189–193. DOI: 10.1038/nature25147.

[2] Cristina Artini. "Crystal chemistry, stability and properties of interlanthanide perovskites: A review". In: *Journal of the European Ceramic Society* 37.2 (2017), pp. 427–440. ISSN: 0955-2219. DOI: https://doi.org/10.1016/j.jeurceramsoc.2016.08.041.

[3] Federico Brivio et al. "Lattice dynamics and vibrational spectra of the orthorhombic, tetragonal, and cubic phases of methylammonium lead iodide". In: *Phys. Rev. B* 92 (14 Oct. 2015), p. 144308. DOI: 10.1103/PhysRevB.92.144308.

[4] R. Hanbury Brown and R.Q. Twiss. "LXXIV. A new type of interferometer for use in radio astronomy". In: *The London, Edinburgh, and Dublin Philosophical Magazine and Journal of Science* 45.366 (1954), pp. 663–682. DOI: 10.1080/14786440708520475.

[5] Marianna D'Amato. *Experimental study of $CsPbBr_3$ perovskite nanocrystals as single photon emitters*. 2020.

[6] Dawei Di et al. "Size-Dependent Photon Emission from Organometal Halide Perovskite Nanocrystals Embedded in an Organic Matrix". In: *The Journal of Physical Chemistry Letters* 6.3 (2015), pp. 446–450. DOI: 10.1021/jz502615e.

[7] Chengjie Ding et al. "Fabrication and characterization of optical nanofiber interferometer and resonator for the visible range". In: *New Journal of Physics* 21.7 (July 2019), p. 073060. DOI: 10.1088/1367-2630/ab31cc.

[8] M. D. Eisaman et al. "Invited Review Article : Single-photon sources and detectors". In: *Review of Scientific Instruments* 82.7 (2011), p. 071101. DOI: 10.1063/1.3610677.

[9] Mark Fox. *Quantum optics : an introduction, volume 15*. OUP Oxford, 2006.

[10] C.et al. Galland. "Two types of luminescence blinking revealed by spectroelectrochemistry of single quantum dots". In: *Nature* 479 (Nov. 2011), pp. 203–207. DOI: https://doi.org/10.1038/nature10569.

[11] Roy J. Glauber. "The Quantum Theory of Optical Coherence". In: *Phys. Rev.* 130 (6 Jan. 1963), pp. 2529–2539. DOI: 10.1103/PhysRev.130.2529.

[12] Son-Tung Ha et al. "Metal halide perovskite nanomaterials: synthesis and applications". In: *Chem. Sci.* 8 (4 2017), pp. 2522–2536. DOI: 10.1039/C6SC04474C.

[13] Fengrui Hu et al. "Superior Optical Properties of Perovskite Nanocrystals as Single Photon Emitters". In: *ACS Nano* 9.12 (2015), pp. 12410–12416. DOI: 10.1021/acsnano.5b05769.

[14] He Huang et al. "Lead Halide Perovskite Nanocrystals in the Research Spotlight : Stability and Defect Tolerance". In: *ACS Energy Letters* 2.9 (2017), pp. 2071–2083. DOI: 10.1021/acsenergylett.7b00547.

[15] Caixia Huo et al. "Optical Spectroscopy of Single Colloidal $CsPbBr_3$ Perovskite Nanoplatelets". In: *Nano Letters* 20.5 (2020), pp. 3673–3680. DOI: 10.1021/acs.nanolett.0c00611.

[16] F. Jelezko and J. Wrachtrup. "Single defect centres in diamond: A review". In: *Physica status solidi (a)* 203.13 (2006), pp. 3207–3225. DOI: https://doi.org/10.1002/pssa.200671403.

[17] Roman Kiselev. "Loss compensation in nanooptical components for lightwave communication". PhD thesis. Sept. 2013. DOI: 10.13140/RG.2.2.26004.04488.

[18] Maksym V. Kovalenko, Loredana Protesescu, and Maryna I. Bodnarchuk. "Properties and potential optoelectronic applications of lead halide perovskite nanocrystals". In: *Science* 358.6364 (2017), pp. 745–750. ISSN: 0036-8075. DOI: 10.1126/science.aam7093.

[19] Li Lang et al. "First-principles study on the electronic and optical properties of cubic ABX3 halide perovskites". In: *Physics Letters A* 378.3 (2014), pp. 290–293. ISSN: 0375-9601. DOI: https://doi.org/10.1016/j.physleta.2013.11.018.

[20] Rodney Loudon. *The quantum theory of light*. OUP Oxford, 2000.

[21] M. Manceau et al. "Effect of charging on CdSe/CdS dot-in-rods single-photon emission". In: *Phys. Rev. B* 90 (3 July 2014), p. 035311. DOI: 10.1103/PhysRevB.90.035311.

[22] G. Murtaza and Iftikhar Ahmad. "First principle study of the structural and optoelectronic properties of cubic perovskites $CsPbM_3$ ($M = Cl$, Br, I)". In: *Physica B: Condensed Matter* 406.17 (2011), pp. 3222–3229. ISSN: 0921-4526. DOI: https://doi.org/10.1016/j.physb.2011.05.028.

[23] Mark Oxborrow and Alastair G Sinclair. "Single-photon sources". In: *Contemporary Physics* 46.3 (2005), pp. 173–206. DOI: 10.1080/00107510512331337936.

[24] Nam-Gyu Park. "Perovskite solar cells: an emerging photovoltaic technology". In: *Materials Today* 18.2 (2015), pp. 65–72. ISSN: 1369-7021. DOI: https://doi.org/10.1016/j.mattod.2014.07.007.

[25] Young-Shin Park et al. "Room Temperature Single-Photon Emission from Individual Perovskite Quantum Dots". In: *ACS Nano* 9.10 (2015), pp. 10386–10393. DOI: 10.1021/acsnano.5b04584.

[26] Stefano Pierini. "Experimental study of perovskite nanocrystals as single photon sources for integrated quantum photonics". PhD thesis. Université de Technologie de Troyes, 2021.

[27] Stefano Pierini et al. “Highly Photostable Perovskite Nanocubes : Toward Integrated Single Photon Sources Based on Tapered Nanofibers”. In: *ACS Photonics* 7.8 (2020), pp. 2265–2272. DOI: 10.1021/acsphotonics.0c00820.

[28] Stefano Pierini et al. *Nanophotonic approaches for integrated quantum photonics*. 2019. arXiv: 1909.10343 [quant-ph].

[29] Loredana Protesescu et al. “Nanocrystals of Cesium Lead Halide Perovskites ($CsPbX_3$, $X = Cl$, Br, and I): Novel Optoelectronic Materials Showing Bright Emission with Wide Color Gamut”. In: *Nano Letters* 15.6 (2015), pp. 3692–3696. DOI: 10.1021/nl5048779.

[30] Gabriele Rainò et al. “Single Cesium Lead Halide Perovskite Nanocrystals at Low Temperature: Fast Single-Photon Emission, Reduced Blinking, and Exciton Fine Structure”. In: *ACS Nano* 10.2 (2016), pp. 2485–2490. DOI: 10.1021/acsnano.5b07328.

[31] Gabriele Rainò et al. “Underestimated Effect of a Polymer Matrix on the Light Emission of Single $CsPbBr_3$ Nanocrystals”. In: *Nano Letters* 19.6 (2019), pp. 3648–3653. DOI: 10.1021/acs.nanolett.9b00689.

[32] S.Pierini et al. “Hybrid devices for quantum nanophotonics”. In: *Journal of Physics: Conference Series* 1537 (May 2020), p. 012005. DOI: 10.1088/1742-6596/1537/1/012005.

[33] M. Sebastian et al. “Excitonic emissions and above-band-gap luminescence in the single-crystal perovskite semiconductors $CsPbBr_3$ and $CsPbCl_3$”. In: *Phys. Rev. B* 92 (23 Dec. 2015), p. 235210. DOI: 10.1103/PhysRevB.92.235210.

[34] Malvin C. Teich and Bahaa E.A. Saleh. “I Photon Bunching and Antibunching”. In: ed. by E. Wolf. Vol. 26. Progress in Optics. Elsevier, 1988, pp. 1–104. DOI: https://doi.org/10.1016/S0079-6638(08)70174-4.

[35] Pooja Tyagi, Sarah M. Arveson, and William A. Tisdale. “Colloidal Organohalide Perovskite Nanoplatelets Exhibiting Quantum Confinement”. In: *The Journal of Physical Chemistry Letters* 6.10 (2015), pp. 1911–1916. DOI: 10.1021/acs.jpclett.5b00664.

[36] Hendrik Utzat et al. “Coherent single-photon emission from colloidal lead halide perovskite quantum dots”. In: *Science* 363.6431 (2019), pp. 1068–1072. ISSN: 0036-8075. DOI: 10.1126/science.aau7392.

[37] Stefano Vezzoli. “Experimental Study of Nanocrystals as Single Photon Sources”. PhD thesis. Paris 6, Jan. 2013.

[38] S. Wahl M.; Orthaus-Müller. “Time tagged time-resolved fluorescence data collection in life sciences; technical note”. In: *PicoQuant GmbH* (2014). Technical note.

[39] Andrei Wenk Hans-Rudolf; Bulakh. *Minerals : Their Constitution and Origin*. New York, NY : Cambridge University Press, 2004.

[40] Ye Yuan et al. “Nature of the band gap of halide perovskites ABX_3 ($A = CH_3NH_3$, Cs B = Sn, Pb $X = Cl, Br, I$): First-principles calculations”. In: *Chinese Physics B* 24.11 (Nov. 2015), p. 116302. DOI: 10.1088/1674-1056/24/11/116302.